Magnetic interpretation in three dimensions using Euler deconvolution

A. B. Reid*, J. M. Allsop‡, H. Granser*,
A. J. Millett§, and I. W. Somerton*

ABSTRACT

Magnetic-survey data in grid form may be interpreted rapidly for source positions and depths by deconvolution using Euler's homogeneity relation. The method employs gradients, either measured or calculated. Data need not be pole-reduced, so that remanence is not an interfering factor. Geologic constraints are imposed by use of a structural index. Model studies show that the method can locate or outline confined sources, vertical pipes, dikes, and contacts with remarkable accuracy. A field example using data from an intensively studied area of onshore Britain shows that the method works well on real data from structurally complex areas and provides a series of depth-labeled Euler trends which mark magnetic edges, notably faults, with good precision.

INTRODUCTION

Magnetic-survey data are routinely interpreted by estimating source depths or locations (Vacquier et al., 1951); consequently, many processing algorithms have been proposed to assist the estimation. Depth estimation is addressed in a statistical sense by Spector and Grant (1970), who exploit the slope of the power spectral density. Boundary location is assisted by calculation of the horizontal gradient of the pseudogravity (Cordell and Grauch, 1985), which peaks over a vertical contact, although the peak is somewhat offset for dipping contacts. The magnitude of the total gradient or analytic signal (Nabighian, 1972, 1974, 1984) peaks directly over a contact with arbitrary dip but is a somewhat noisy estimator (Hansen et al., 1987). The breadth of the peak allows estimation of the depth to the source. All the above methods may be applied to either gridded data or profiles.

A number of automatic profile processing methods (reviewed by Thompson, 1982) combine source location and depth estimation. Werner deconvolution (Hartman et al., 1971; Jain, 1976) fits elementary models to successive segments of a profile and estimates source location, depth, and dip. A similar approach is followed by Naudy (1971), who employs prism and thin-plate models. Thompson (1982) describes a method which applies Euler's equation to successive segments of a pole-reduced profile, solves for source position, and obtains an indication of source type.

Despite this very considerable body of methods, there remains a need for a fast means of processing a magnetic grid to derive trends and depth estimates in an automatic or semiautomatic manner. Thompson (1982) suggests in passing that a 3-D implementation of his EULDPH algorithm could be used to analyze mapped magnetic data. We discuss such an implementation.

THEORY

Thompson (1982) showed that Euler's homogeneity relation could be written in the form

$$(x - x_0)\partial T/\partial x + (y - y_0)\partial T/\partial y$$
$$+ (z - z_0)\partial T/\partial z = N(B - T), \qquad (1)$$

where (x_0, y_0, z_0) is the position of a magnetic source whose total field T is detected at (x, y, z). The total field has a regional value of B.

The degree of homogeneity N may be interpreted as a structural index (SI) (Thompson, 1982), which is a measure of the rate of change with distance of a field. Thus, the magnetic field of a point dipole falls off as the inverse cube, giving an index of three, while an effective vertical line source such as a narrow, vertical pipe gives rise to an inverse square field falloff and an index of two. Extended bodies are

assemblages of dipoles and have indices ranging from zero (infinite sheet) to three.

While the structural index for the dipole may be regarded as obvious from elementary considerations, we are not aware of derivations of the indices for extended bodies. It is shown in the Appendix that the magnetic field of a thin, infinitely deep dipping dike or sheet edge exhibits an index of 1.0, as shown empirically by Thompson (1982). A finite density step gives a gravity anomaly that also exhibits an SI of 1.0 and depth estimates approximately locate the midpoint of the step.

Thompson (1982) suggests that the index for a magnetic contact is less than 0.5. This value leads to underestimates of depth, even when testing ideal models. As shown in the Appendix, the value for a sloping contact is, in fact, zero, provided that an offset A is introduced. The appropriate form of Euler's equation is then

$$(x - x_0)\partial T/\partial x + (y - y_0)\partial T/\partial y + (z - z_0)\partial T/\partial z = A,$$
(2)

where A incorporates amplitude, strike, and dip factors which cannot be separated easily (see the Appendix).

SOLUTION STRATEGY

The 3-D forms of Euler's equation [either equation (1) or equation (2)] are easily applied to gridded data. The steps in the process are the following:

(1) Calculate (or measure) the gradients $\partial T/\partial x$, $\partial T/\partial y$, $\partial T/\partial z$.

(2) Locate a square window within the grids of gradient values and field values of size 3 × 3 grid points or greater. A 10 × 10 window produces good results and is acceptably fast, but high-resolution data yield good results with smaller windows.

(3a) For each desired nonzero structural index, use all points in the window to solve Euler's equation (1) for a source position (x_0, y_0, z_0) and a background value B using Moore-Penrose inversion (Lawson and Hanson, 1974) to obtain least-squares estimates. A 10 × 10 window provides 100 equations, from which the four unknowns and their uncertainties (standard deviations) are obtained. Record the solution if the depth uncertainty is less than, say, 15% of the calculated depth.

(3b) For a structural index of zero, proceed as for (3a), but use equation (2) and solve for source position and the arbitrary offset value A.

(4) Repeat steps (2) and (3) for some or all possible window positions, including overlaps.

(5) Plot maps of the solutions, one for each structural index. Each solution is plotted at its plan (x, y) position using a symbol size proportional to depth z. This display method was adopted because it is easily implemented, cheaply printed, and readily understood.

MODEL STUDIES

Figure 1 shows the successful application of Euler deconvolution to model fields derived from a sphere (point dipole;

Figure 1a), intrusive pipe (vertical line source; Figure 1b), thin dike (Figures 1c and 1d), contact (Figure 1e), and irregular sill (Figure 1f), covering the full structural index range. The results are summarized in Table 1. In all cases where the appropriate structural index was used, the model is clearly delineated and the estimated depth is close to the model value.

Choice of structural index

The thin-dike anomaly was deconvolved using two indices to show that use of the wrong index yields scattered solutions and biased depths (Figure 1d). An index that is too low gives depths that are too shallow; one that is too high gives estimates that are too deep. But even if the index is correct, it is clear that depth estimates are more precise for high-index sources than for low (Table 1). Despite the scattered result and overestimated depth for the dike deconvolved with index of 2.0, the dike trend is still evident, suggesting that gross structural trends can still be outlined, despite a poor choice of the index.

Although the structural-index approach to source description does not include irregular boundaries, each solution employs only data within its window, so that irregular sill-like bodies can be well delineated by the Euler method with an index of 1.0, while irregular contacts are well shown with a zero index. The irregular-sill model (Figure 1f) shows well-outlined curve boundaries and also shows that solutions cluster where model curvature is high.

A real data set is likely to contain anomalies from sources with various structural indices. It is, therefore, necessary to solve for a range of indices (say 0.0, 0.5, and 1.0) and to plot the results for each index. The maps are then examined feature by feature and the index which gives the best solution clustering is chosen for each feature. This procedure also gives some clue as to the nature of the feature. Thus, a sill edge, dike, or fault with limited throw is best displayed at an index of 1.0, while a fault with large throw may be best displayed at a zero index. Intermediate cases are best shown by an index of 0.5. The field example shows different features clustering at different indices.

Pole reduction and dip estimation

Thompson (1982) prefers to work with pole-reduced data on the ground that more accurate depth estimates are obtained, but our own model studies and theoretical work lead to a different conclusion. The dike and contact models are vertical, whereas the irregular sill is horizontal. All the models are in a nonvertical field and have arbitrary or varying strikes. Although no pole reduction has been applied, the source positions are nevertheless accurately reproduced. It is shown in the Appendix that the results are independent of field direction, dip, or strike of the magnetic feature. It, therefore, appears that pole reduction prior to Euler deconvolution is unnecessary. The method may be expected to yield useful results with data collected from regions of horizontal or near-horizontal magnetic field. It should also yield useful results in the presence of remanence. The corollary is that the method cannot and does not yield any dip information. Dips must be estimated by other means (e.g., Gay, 1963) if they are required.
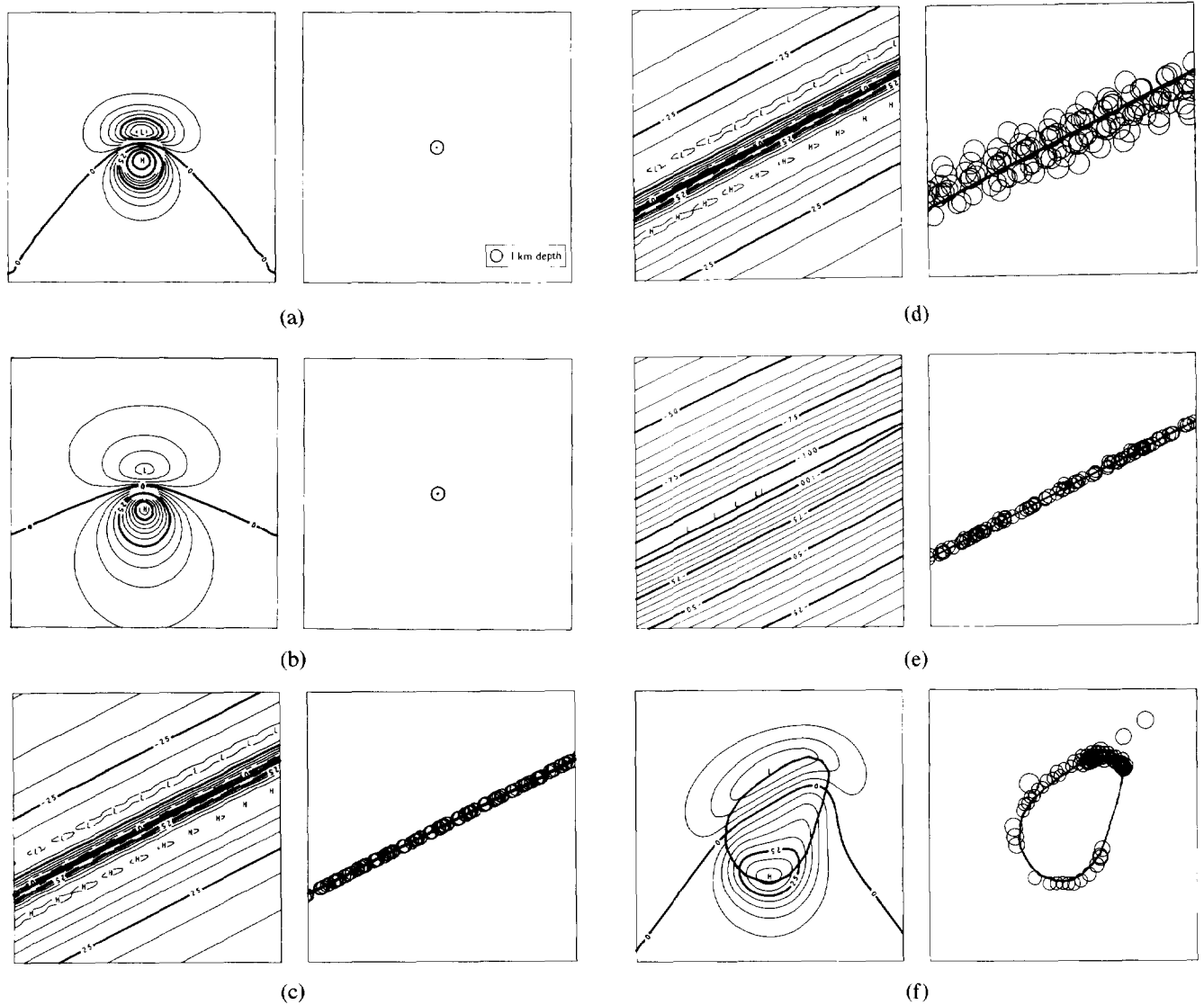
FIG. 1. Model results. All models have magnetization induced by a field with inclination at 45° and depth to top of 1 km. For each pair, magnetic-field contours from the model are shown on left, Euler deconvolution on right with circle diameter proportional to calculated depth. Grid interval is 250 m. Plotted area is 10 × 10 km. (a) Sphere, structural index 3. (b) Vertical pipe, structural index 2. (c) Vertical dike, structural index 1. (d) Vertical dike, out of focus, and shown too deep by structural index 2. (e) Contact, structural index zero. (f) Irregular sill, structural index 1.

Table 1. Modeling results. All models at 1000 m depth.

Model	Structural index	Window size (grid points)	Acceptance level	No. of solns	Euler depth (m)	Results
Sphere	3	4 × 4	0.4%	86	1000.7 ± 2.1	Excellent
Vert. pipe	2	4 × 4	0.4%	84	998.0 ± 2.5	Excellent
Dike	1	4 × 4	0.3%	98	994.4 ± 1.3	Good
Dike	2 (wrong index)	4 × 4	3.0%	181	1488 ± 89	Poor
Contact	0	4 × 4	4.0%	246	1012 ± 252	Fair
Sill	1	3 × 3	2.2%	87	1010 ± 128	Fair

Note—Solutions are accepted if the uncertainty is less than a specified percentage of the calculated depth (the acceptance level).

Selection criteria and spurious solutions

Our method employs overlapping windows and produces a solution for every window, so that the total number of solutions can approach the number of grid points. Where a window does not include any significant gradients or where it includes gradients arising from several sources, the solution has a high uncertainty. Noisy or poorly gridded data sets also affect the solution statistics by degrading the fit. In addition, we observe that the lower the structural index employed, the worse the precision, even when the index used is the appropriate one. This is the case for both model and real data (see Tables 1 and 2). Lower indices are associated with lower gradients and curvatures (for a given depth) and typically these have lower relative precisions, being calculated by difference. It is, therefore, not unreasonable that parameters derived from these lower precision data are also less precisely obtained. The choice of acceptance level is empirical.

If the selection level is set too strictly, some reliable depth estimates are obtained; but some structures are poorly delineated because there are few solutions. If the level is set too loosely, structures such as contacts are surrounded by a cloud of poorly defined solutions which obscure the better solutions. In practice, some undesired, scattered solutions are accepted for the sake of defining as many structures as possible. The irregular-sill model (Figure 1f) shows the problems well. The model simultaneously displays a few scattered solutions and regions where no solutions are obtained, even though they might be expected. The field example also shows these effects.

FIELD EXAMPLE

The study area, located in central England (Figure 2), consists of a portion of the Birmingham to Oxford "ridge"—an uplifted block with shallow magnetic sources coinciding with Paleozoic folds, producing high-amplitude magnetic anomalies, flanked by fault-bounded basins on the west and northeast. Figures 3a and 3b, extracted from Smith et al. (1985), show the most accessible published information on the deep geology of the area, which was chosen because it has recently been the subject of considerable research (Chadwick, 1985; Chadwick and Smith, 1988; Cornwell and Allsop, 1988). The sense of faulting is shown differently on Figures 3a and 3b but is reproduced from the published originals. As seen below, that shown in Figure 3b is preferred. The gravity data (Figure 3c) were made available by the British Geological Survey (BGS). They support the interpreted thickening of younger strata in the SW and NE shown in Figures 3a and 3b. The aeromagnetic data (Figure 3d), also supplied by the BGS, show strong gradients and anomaly closures due to a variety of sources from outcrop to depths greater than 5 km. Figure 4 shows the location of independent geologic and geophysical information used for comparison with the aeromagnetic data.

The aeromagnetic survey was flown in 1955 at a line spacing of 2 km and ground clearance of 550 m using analog recording. The measurements were recently made available in machine-readable form by digitizing the 10 nT contour intersections of the flight lines, plus some intermediate points on the original 1:63 360 worksheets. They were gridded at a 1 km interval and subjected to Euler deconvolution using the structural indices, window sizes, and selection criteria shown in Table 2. The results are shown in Figures 5a–5c, whereas Figure 5d shows a structural interpretation based on the deconvolution. The remainder of this section compares the interpretation (and the source depths implied by the symbol sizes) with independent evidence.

Independent data available

Four basic types of control data were used to obtain or estimate depths to magnetic and nonmagnetic basement and, where possible, to define the type of basement, its physical properties, geologic description, structure, and age. The term "magnetic basement" is used here to denote pre-Carboniferous rocks which, in this area, include basalts and tuffs (Poole, 1977). Even where igneous rocks are not present, pre-Carboniferous rocks are considered unlikely sources or repositories of coal or other hydrocarbons and are termed "nonmagnetic basement." The control data types were

> (a) borehole information,
> (b) seismic reflection surveys,
> (c) gravity surveys and ground and aeromagnetic data interpreted using other methods, and
> (d) resistivity data.

Borehole information was available from 158 holes (Figure 4); although 18% of these holes did not intersect pre-Permian rocks, they did give useful minimum depth estimates in areas of deep basement, such as the Worcester graben (Whittaker et al., 1980). They also provided physical property data and assisted in the identification of seismic reflectors on BGS seismic lines and on commercial records interpreted by the Deep Geology Research Group (DGRG) within the BGS. The seismically derived depths were particularly useful in the Worcester graben (Chadwick, 1985; Chadwick and Smith, 1988) and Bicester areas and on the eastern side of the Warwickshire Coalfield (Figure 5d; Allsop, 1981; Cornwell and Allsop, 1988).

Gravity and magnetic interpretations (Allsop, 1981; Cornwell and Allsop, 1988; Taylor and Rushton, 1971) were supplemented by detailed ground magnetic and gravity traverses (Figure 4; Cornwell and Allsop, 1979). In the study area, 17 Wenner expanding probe resistivity traverses (Figure 4, maximum "a" spacing 800 m) provided estimates of depth to basement (Allsop, 1988), mainly in the area of the SW-NE trending Charlton anticline (Figure 5d). Finally, detailed contour maps of the Mesozoic sediments (Whittaker, 1985) and maps of the pre-Permian paleogeology and contours (Figures 3a, 3b; Smith et al., 1985) were available as a published summary of the geology and structure of the area.

Interpretation

The Euler deconvolution maps (Figures 5a–5c) present the derived source positions as circles at their plan positions with depth proportional to diameter. They show roughly the same trends at all three structural indices, but with different degrees of clustering and different depths.

The correct index for any given feature was chosen as that

which gave the tightest clustering, when this could be distinguished. For example, the short linear feature trending NNE at grid position (415^{000}, 227^{000}) shows best clustering using index 0.5 and is therefore taken to have a depth of 1–2 km (given by the symbol size on Figure 5b). It is likely to be a subsidiary fault with vertical displacement of 1 km or less, suggested by its index. The curved feature most clearly seen using 1.0 (Figure 5c) passing through Banbury at grid position (445^{000}, 240^{000}) is likely to be a feature of little depth extent whose top is at a depth of about 1.5 km within the Carboniferous section, possibly the edge of a volcanic layer. A similar Euler approach was applied to all the features shown, together with reference to the contour maps (Figures 3c, 3d), to arrive at a subsurface integration. The results were classified by comparison with the independent information described above and the interpretation summarized in Table 3. The final interpretation is shown in Figure 5d.

Known features well represented.—The known boundary faults to the east and west of the Central block (Smith, 1987; Chadwick and Smith, 1988; Whittaker et al., 1980) are the most obvious features on the Euler maps and are represented in all three deconvolutions (Figures 5a–5c). The western boundary fault is shown as a complex fault zone on the 0.5 index Euler map (Figure 5b), which indicates a westward increase in depth to magnetic basement from about 2 km over the Central block to 2.5–3.5 km through the fault zone. Within the southern Worcester graben, the maximum depth to magnetic sources is about 6 km (Figures 5b, 5c), although there are very few acceptable solutions in this area. The seismic-reflection evidence (Chadwick, 1985;

Chadwick and Smith, 1988) suggests that such sources lie within the Precambrian.

The eastern flank of the Central block is also evident on the Euler maps, defining the Eastern Boundary fault of the Warwickshire Coalfield (Figure 5d), but the faulting appears to be less dramatic than in the west. The Euler solutions on the 0.5 index map provide depths within 0.3 km of the depth estimates obtained by other means (Allsop, 1981; Cornwell and Allsop, 1988; Taylor and Rushton, 1971).

Known features poorly represented.—The northern and central sections of the Central block are not well delineated on the Euler plots (Figure 5). The large areas, devoid of depth estimates, are surprising, since a number of features appear on the magnetic contour map. The lack of Euler solutions may be due to interference between several neighboring anomalies. The sparseness of data points compared with the complexity of the contours in this area (Figure 3d) suggests that the field may be undersampled here.

The SW to NE boundary fault dividing the central from the southern section of the Central block (Figure 5d) separates contrasting igneous rocks proved in the Withycombe Farm borehole (443^{000}, 240^{000}; Poole, 1978) in the central section of the Central block from those in the Steeple Aston borehole (447^{000}, 226^{000}; Poole, 1977) in the southern section. This boundary is poorly defined by the Euler solutions, although there is some indication of its trend, and sources are shown to be deeper to the south of the fault than to the north (Figures 5a–5c). The fault does not disturb the base of the Permian section significantly (Figure 3b) and may be poorly represented because it does not juxtapose rocks having significant magnetization contrast.

Previously suspected features confirmed.—Volcanic rocks within the Silurian and Ordovician strata have been intersected in the Steeple Aston borehole and in the Bicester borehole (458^{000}, 221^{000}) within the Charlton anticline (Figure 5d). Ground magnetic and gravity surveys (Cornwell and Allsop, 1979, Figure 4) show that the volcanics extend for some way within the southern section of the Central block. The scattered Euler solutions obtained with all indices in this area (Figures 5a–5c) confirm the suspicion that the volcanics extend well beyond the ground surveyed area. The absence of such scattered solutions north of the boundary fault between the Withycombe Farm and Steeple Aston boreholes suggests that the volcanics are confined to the southern section.

Previously unrecognized, geologically reasonable features.—A series of Euler solutions branches away southwestward from the Eastern Boundary fault at (443^{000}, 262^{000}; Figures 5a–5c). Since this feature seems best defined using an index of 0.5, it could be a fault of moderate throw. The gravity map (Figure 3c) shows some detail in this area, supporting the suggestion of structural complexity.

At the "hinge point" (418^{000}, 225^{500}; Figure 5d) and to the south, where three possible faults converge, there appears a deep cluster of Euler solutions (Figures 5a–5c), consistent with a magnetic source at a depth of about 10 km. This body could be similar to the postulated diorites at Abingdon
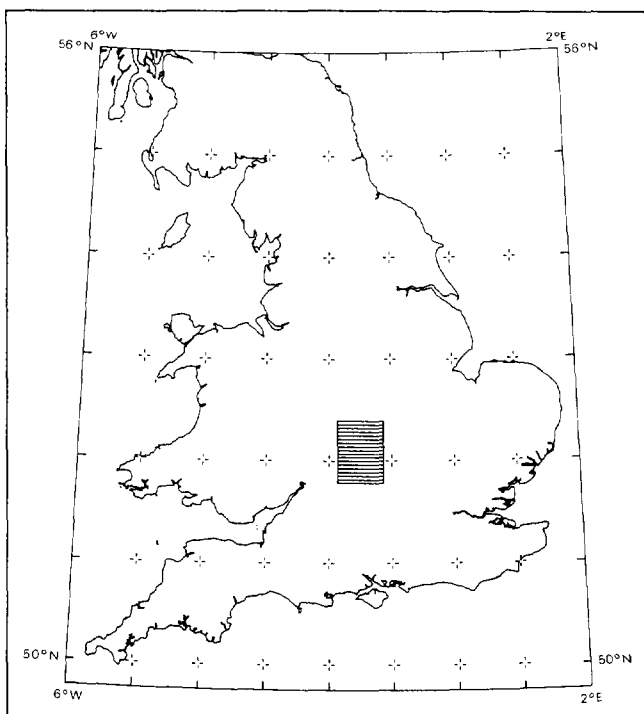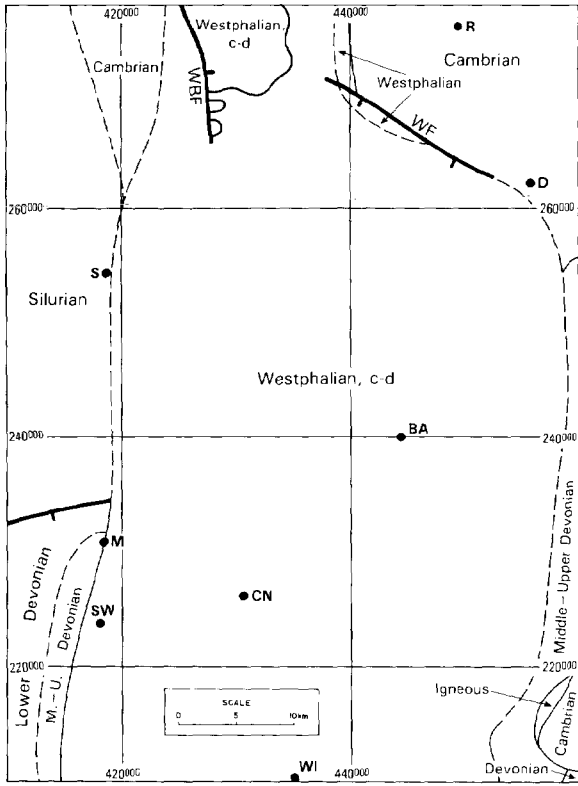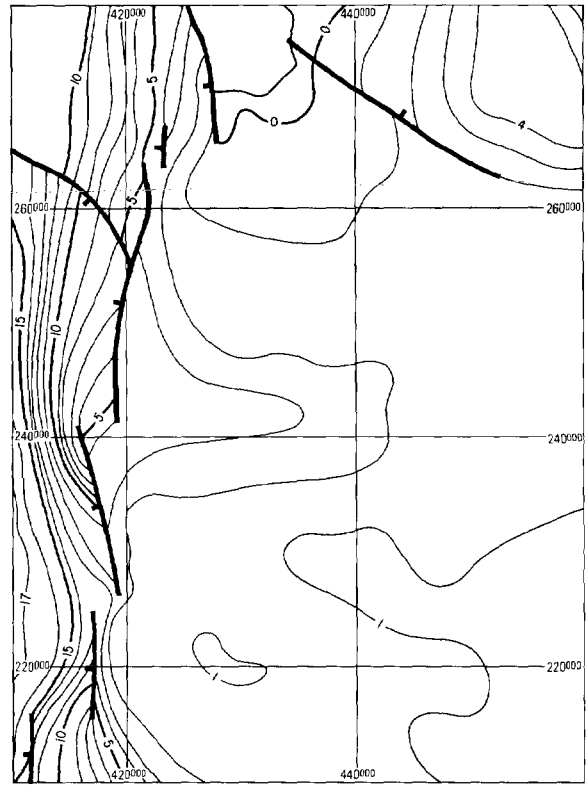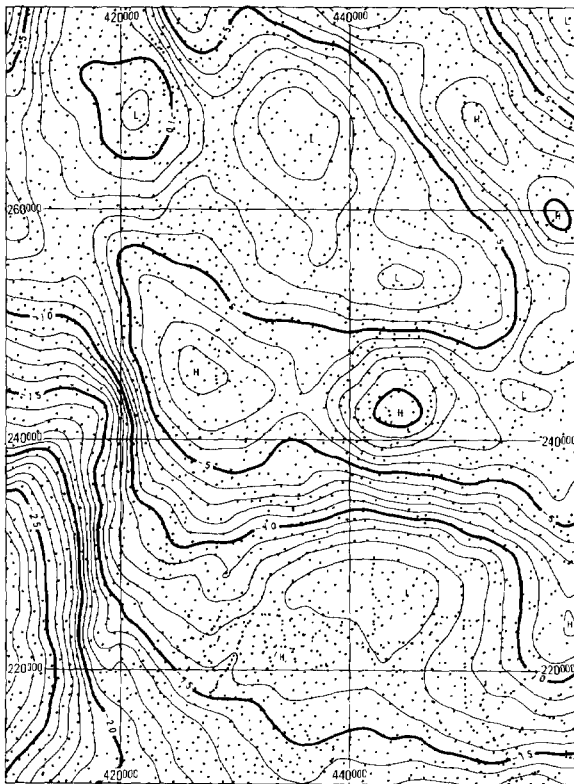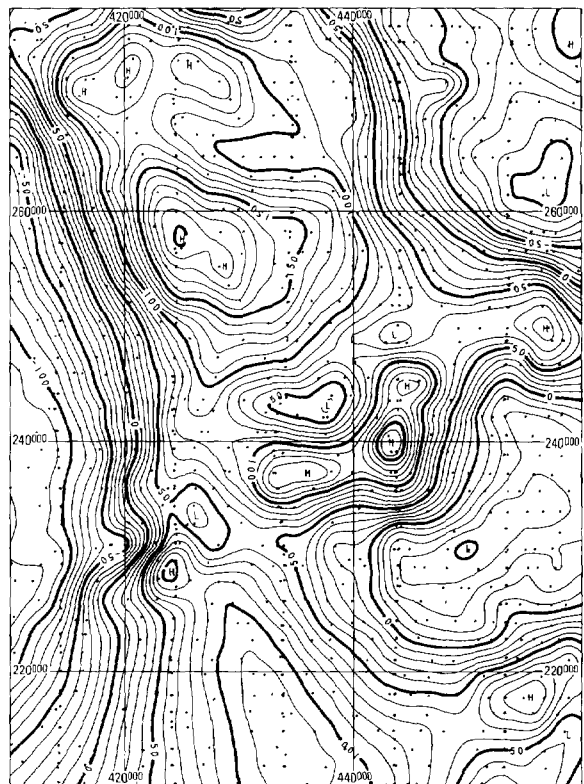

FIG. 2. Field study location in south-central England.

(a)

(b)

(c)

(d)

$(448^{000}, 198^{000})$ and Reading/Newbury $(445^{000}, 177^{000})$ south of the study area (Ellis and Kearey, 1984).

On the 1.0 index map (Figure 5c) there is a series of Euler solutions which may indicate thin irregular magnetic bodies at depths between 2 and 3 km radiating west and south from the hinge point (Figure 5d) into the Worcester graben. Comparison with Figure 3b shows that the postulated bodies are deeper than the Permian section and could therefore be lavas within the pre-Carboniferous basement, since Siluro-Ordovician basalts and tuffs are reported from the Steeple Aston borehole (Poole, 1977).

Apparently spurious features.—There are some isolated Euler solutions at unlikely depths, notably in the extreme
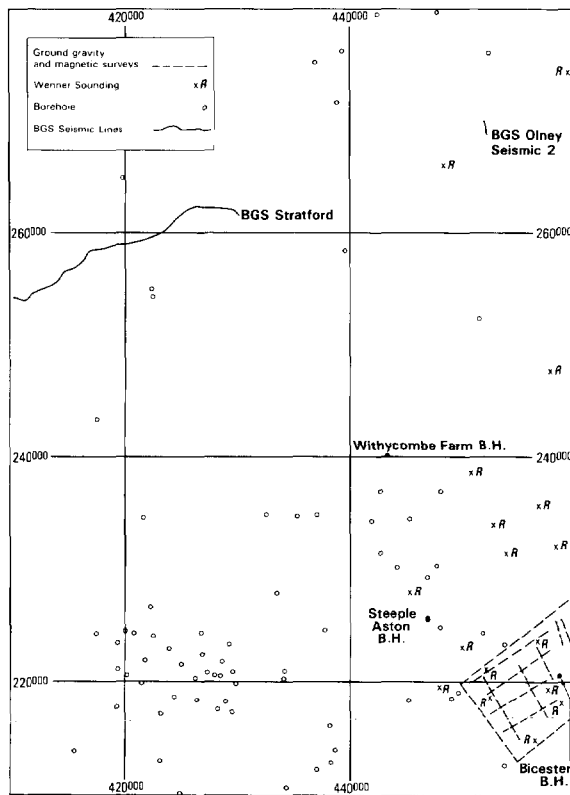

FIG. 4. Location of borehole, seismic reflection, resistivity, and detailed gravity and ground magnetic data.

FIG. 3. (Opposite) (a) Geologic map of pre-Permian subcrop and outcrop (after Smith et al., 1985). Location using British National Grid. BA—Banbury, CN—Chipping Norton, D—Daventry, M—Moreton-in-the-Marsh, R—Rugby, S—Stratford-upon-Avon, SW—Stow-on-the-Wold, WI-Witney, WBF—Western Boundary Fault. WF—Warton fault. (b) Depth contours w.r.t. mean sea level on pre-Permian surface (contour interval 0.1 km, after Smith et al., 1985). (c) Bouguer anomaly map (contour interval is 1 mGal; grid interval is 1 km, station positions shown as dots. (d) Aeromagnetic field with geomagnetic reference field removed (contour interval is 10 nT; grid interval is 1 km), digitized points shown as dots.

Table 2. Parameters used in Euler deconvolution of field data.

Structural index	Window	Acceptance level
0.0	10 × 10	25%
0.5	10 × 10	18%
1.0	10 × 10	15%

northeast $(455^{000}, 270^{000}$; Figures 5a–5c), where the solutions conflict with seismic and gravity evidence of thick sediments. They are probably artifacts of the method.

DISCUSSION

Grid and data quality

Since equations (1) and (2) involve field values and their gradients in gridded form, the method is clearly dependent on the reliability of those values and gradients. Reliability in turn depends on the acquisition parameters, data processing methods, and gridding technique used.

Reid (1980) discusses the choice of acquisition parameters and gives criteria based on the sampling theorem and the phenomenon of aliasing. The specification of flying height, profile spacing, and sample spacing involves consideration of the required resolution and the anticipated depth to sources of interest; but the profile spacing should not exceed the depth to sources of interest if the calculated or measured gradients are to be a reliable representation of the real gradients, especially at the shorter wavelengths. The data reduction should eliminate any significant leveling or location errors. Because aliasing, leveling, and location errors mostly affect shorter wavelengths, data quality can sometimes be improved by judicious low-pass filtering (e.g., upward continuation) at the expense of resolution and of the representation of the effects of shallower sources. If the data are of poor quality, it may be expected that, with this or any other method, the shallowest sources will be misrepresented, totally missed, or reported at an exaggerated depth.

A grid interval greater than the along-profile sample spacing but less than the profile spacing is normally chosen. For most gridders, this choice implies some along-profile averaging and some across-profile interpolation. If the survey criterion above is honored, neither of these should cause serious errors; but the grid will be least reliable between flight lines.

The Euler deconvolution technique offers a means of incorporating any available gradient survey data directly into an interpretation. Since both low-level noise and poor data quality in the original total field data are amplified when gradients are calculated, the use of measured rather than calculated gradients should improve the results substantially. If three-component measured gradients were available, it would be possible to apply Euler deconvolution to the data directly and avoid the gridding step.
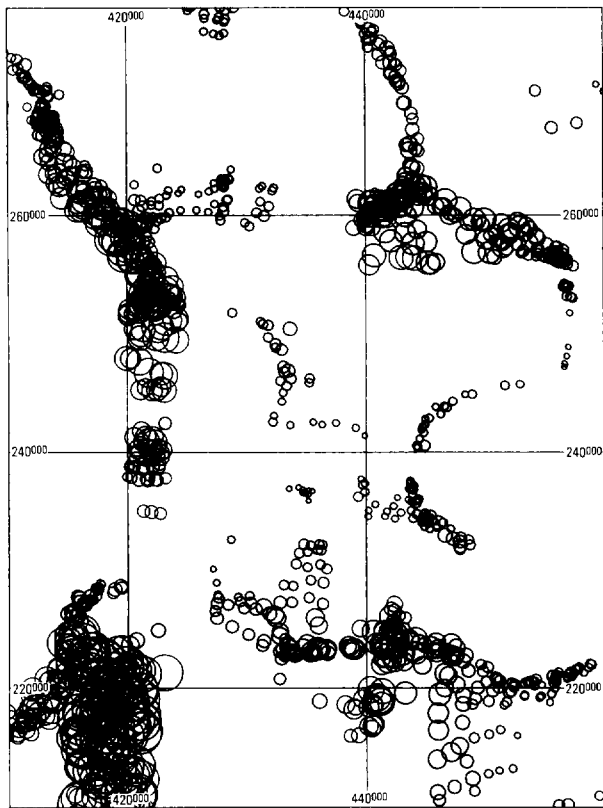
Choice of window size—Interfering sources

If the grid is representative of the anomalies present, but anomalies arising from different sources are so close together that they both occupy any given window, poor fit statistics cause the solution to be rejected, as was seen in the
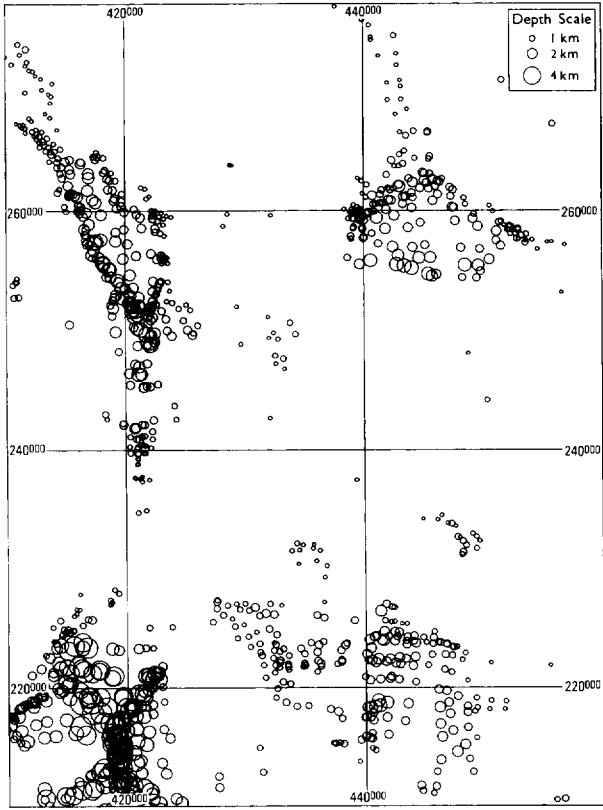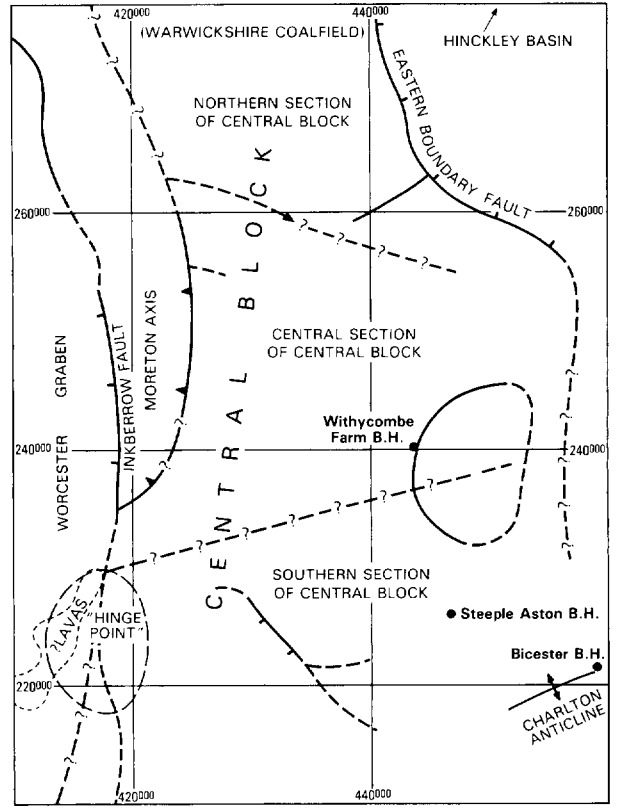
(a)
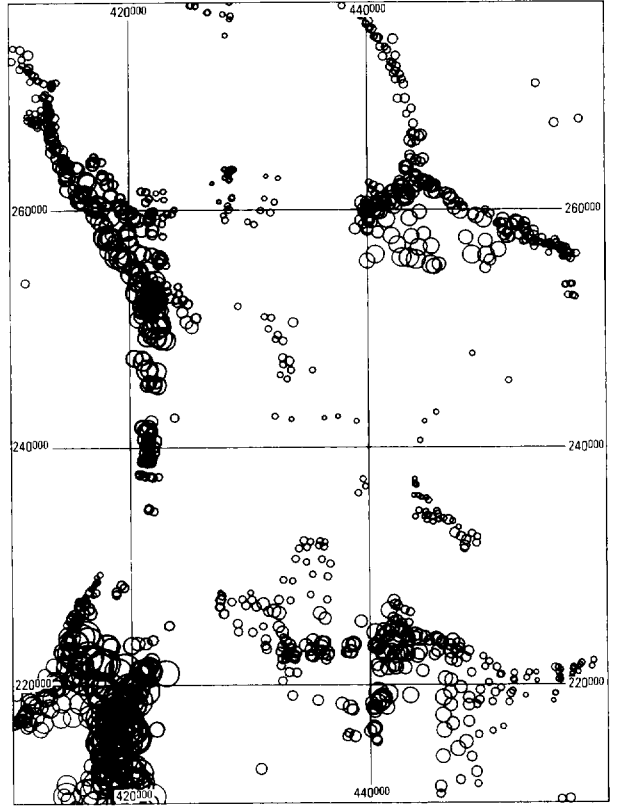
(b)

(c)

(d)

Table 3. Summary of geologic and geophysical interpretation, incorporating all available information.

(1) Central block

NNW-SSE "ridge" with closely spaced, high-amplitude magnetic anomalies (200 nT average). Local variations—magnetic sources in Paleozoic folds. Magnetic and gravity trends often near-coincident. Magnetic basement varies from outcrop to 1.5 km. Block subdivided into three sections by major faults (Smith, 1987; Whittaker, 1985).

   (a) **Northern section** Lamprophyre sills (outcrop) and Carboniferous volcanics are nonmagnetic. Magnetic basement within Precambrian below 1.0 km. General ESE-WNW aeromagnetic gradients (fault-trends).

   (b) **Central section** (Withycombe Farm). Separated from the north by NW-SE fault. High-amplitude magnetic anomalies with general WSW-ENE trends—possibly Precambrian diorites and basalts. Intervening "lows"—possible Devonian sediments. Southern boundary—major NE-SW fault between Withycombe Farm and Steeple Aston boreholes.

   (c) **Southern section** High-amplitude magnetic anomalies. Shallow Siluro-Ordovician basalts and tuffs (Steeple Aston Borehole). ENE-WSW trends—Charlton anticline at Bicester (dolerite and tuffs). Magnetic basement from near surface to 1.0 km with intervening pockets of Devonian sediments.

(2) Worcester graben (on western flank of Central block).

Central magnetic "low" of about -230 nT with major faults against Central block. Graben: 2 to 3 km of post-Precambrian sediments (deepest in east). In NE, fault complex includes large thrust and normal Inkberrow fault, in the area of Vale of Moreton Axis. "Hinge point" $(418^{000}, 225^{500})$—junction of eastern boundary fault of Worchester graben and fault between south and central sections of Central block.

(3) Warwickshire-Charnwood "low" (on northeastern flank of Central block)

Eastern boundary fault of Warwickshire Coalfield—strong gravity and magnetic gradients. Hinckley basin (>1.5 km of Permo-Triassic sediments—Allsop and Arthur, 1983; Cribb, 1975).

---

field example. There is, therefore, reason to keep the window as small as possible. On the other hand, broad anomalies arising from deep sources are poorly represented in a small window; and unreliable estimates of depth and position of source are likely.

Simple models may be deconvolved with windows as small as 3×3 grid points, but real data are best deconvolved with bigger windows, ranging from 6×6 (to delineate shallow sources such as intrasedimentary volcanics) to about 20×20 (for very deep basement sources and the Curie point isotherm). Minimum depths returned are about the same as the grid interval. Maximum depths are about twice the window size. The models were examined using 3×3 or 4×4 windows, a grid interval of 250 m, and source depths of 1 km (Table 1). The field example used 10×10 windows and a grid interval of 1 km.

Computational efficiency

Euler deconvolution is particularly useful for the rapid examination of large data sets, but it is computer-intensive. For each structural index and at each point in the grid, 100 observation equations (typically) are used to estimate four unknowns and their standard deviations. Grids are frequently too large to be stored in fast memory, but they must be accessed window by window rather than column by column. We have achieved acceptable processing times on a minicomputer (Prime 550) for large data sets and have

implemented the algorithm for modeling purposes on a personal computer.

CONCLUSION

Euler deconvolution is both a boundary finder and a depth estimator. Some indication of the source type may be gained by varying the structural index for any particular feature. Euler deconvolution extracts information from a grid which is otherwise hard to interpret in a contour map. The most important products are the delineation of trends such as basement faults and estimates of their depths.

The gravity anomalies of some geologic features also obey Euler's equation (see the Appendix for an example). The method can be expected to provide useful information about faults and steeply dipping contacts and basin edges where density contrasts exist. The method should be directly applicable to gravity gradiometer measurements.

The structural index for a magnetic contact of infinite depth extent has been shown in the Appendix to be zero. An infinite depth extent is approximated by finite structures where the depth to the lower limit of the structure is several times the depth to the upper. We observe, however, that real faults are typically complex structures, so that slightly higher indices are often appropriate. Useful structural indices for gravity anomalies are likely to lie in the range from zero to unity.

FIG. 5. Euler deconvolution of the aeromagnetic data. Source depth is indicated by circle diameter. (a) Structural index 0.0. (b) Structural index 0.5. (c) Structural index 1.0. (d) Structural interpretation of Eular trends.

ments in the paper. It has come to our notice that early unpublished work on the method was done by Sheldon Breiner. We thank him for his encouragement of our own work.

We are grateful to Dr. A. Whittaker and the members of the Deep Geology Research Group of the British Geological Survey for the compilation of geologic and geophysical test data and to Dr. R. T. Haworth (Chief Geophysicist) for his assistance in the final compilation of the assessment. We are also indebted to the BGS for provision of the primary test data set.

This paper is published with the approval of the Directors of The Robertson Group plc. and the Director, British Geological Survey (Natural Environment Research Council).

REFERENCES

Allsop, J. M., 1981, Geophysical appraisal of some geological problems in the English Midlands: Rep. Deep Geol. Unit, Inst. Geol. Sci., 10.
—— 1988, Deep resistivity surveys in the English Midlands: Rep. Deep Geol. Res. Group, Brit. Geol. Surv. 88/10.
Allsop, J. M., and Arthur, M. J., 1983, A possible extension of the South Leicestershire Diorite Complex: Rep. Inst. Geol. Sci., 83/10, 25–30.
Am, K., 1972, The arbitrarily magnetized dike: interpretation by characteristics: Geoexpl., 10, 63–90.
Bosum, W., 1968, Ein automatisches Verfahren zur Interpretation magnetischer Anomalien nach der Methode der kleinsten Quadrate: Geophys. Prosp., 16, 107–126.
Chadwick, R. A., 1985, Seismic reflection investigations into the stratigraphy and structural evolution of the Worcester Basin: J. Geol. Soc. London, 142, 187–202.
Chadwick, R. A., and Smith, N. J. P., 1988, Evidence of negative structural inversion beneath central England from new seismic reflection data: J. Geol. Soc. London, 145, 519–222.
Cordell, L., and Grauch, V. J. S., 1985, Mapping basement magnetization zones from aeromagnetic data in the San Juan basin, New Mexico, in Hinze, W. J., Ed., The utility of regional gravity and magnetic anomaly maps: Soc. Expl. Geophys., 181–197.
Cornwell, J. D., and Allsop, J. M., 1979, Geophysical investigation of the South Midlands basement: 2—detailed magnetic surveys: Rep. Appl. Geophys. Unit, Inst. Geol. Sci., 10.
—— 1988, Geophysical investigations, in Worssam, B. C., and Old, R. A., Eds., Geology of the country around Coalville: Mem. Brit. Geol. Surv., Sheet 155, 113–122.
Cribb, S. J., 1975, Rubidium-strontium ages and strontium isotope ratios from the igneous rocks of Leicestershire: J. Geol. Soc. London, 131, 203–212.
Ellis, P. F., and Kearey, P., 1984, An investigation of the Reading-Newbury magnetic anomaly: J. Geol. Soc. London, 141, 349–356.
Gay, S. P., 1963, Standard curves for interpretation of magnetic anomalies over long tabular bodies: Geophysics, 28, 161–200.
Hansen, R. O., Pawlowski, R. S., and Wang, X., 1987, Joint use of

analytic signal and amplitude of horizontal gradient maxima for three-dimensional gravity data interpretation: 57th Ann. Internat. Mtg., Soc. Expl. Geophys., Expanded Abstracts, 100–102.
Hartman, R. R., Teskey, D. J., and Friedberg, J. L., 1971, A system for rapid digital aeromagnetic interpretation: Geophysics, 36, 891–918.
Jain, S., 1976, An automatic method of direct interpretation of magnetic profiles: Geophysics, 41, 531–541.
Jung, K., 1961, Schwerkraftverfahren in der angewandten Geophysik: Geest und Portig.
Lawson, C. L., and Hanson, R. J., 1974, Solving least squares problems: Prentice-Hall Inc.
Nabighian, M. N., 1972, The analytic signal of two-dimensional magnetic bodies with polygonal cross-section: its properties and use for automated anomaly interpretation: Geophysics, 37, 507–517.
—— 1974, Additional comments on the analytic signal of two-dimensional magnetic bodies with polygonal cross section: Geophysics, 39, 85–92.
—— 1984, Toward a three-dimensional automatic interpretation of potential field data via generalized Hilbert transforms: Fundamental relations: Geophysics, 49, 780–786.
Naudy, H., 1971, Automatic determination of depth on aeromagnetic profiles: Geophysics, 36, 717–722.
Poole, E. G., Ed., 1977, Stratigraphy of the Steeple-Aston Borehole, Oxfordshire: Bull. Geol. Surv. Great Britain, 57.
—— 1978, Stratigraphy of the Withycombe Farm Borehole, near Banbury, Oxfordshire: Bull. Geol. Surv. Great Britain, 68.
Reid, A. B., 1980, Aeromagnetic survey design: Geophysics, 45, 973–976.
Smellie, D. W., 1956, Elementary approximations in aeromagnetic interpretation: Geophysics, 21, 1021–1040.
Smith, N. J. P., 1987, The deep geology of central England: the prospectivity of the Paleozoic rocks, in Brooks, J., and Glennie, K., Eds., Petroleum geology of north west Europe: Graham and Trotman, 2, 217–224.
Smith, N. J. P., Allsop, J. M., Chadwick, R. A., Holliday, D. W., Holloway, S., Kirby, G. A., Armstrong, E. J. J., Auld, H. A., Bulat, J., Jackson, D. I., Jones, S. M., Mulholland, P., Oates, N. K., Quinn, M. F., Swallow, J. L., and Bennett, J. R. P., 1985, Map 1—Pre-Permian surface of the U.K. (south): Brit. Geol. Surv. Map 2—Contours of the top of the pre-Permian surface of the U.K. (south): Brit. Geol. Surv.
Spector, A., and Grant, F. S., 1970, Statistical models for interpreting aeromagnetic data: Geophysics, 35, 293–302.
Taylor, K., and Rushton, A. W. A., 1971, The pre-Westphalian geology of the Warwickshire Coalfield: Bull. Geol. Surv. Great Britain, 35.
Thompson, D. T., 1982, EULDPH—A new technique for making computer-assisted depth estimates from magnetic data: Geophysics, 47, 31–37.
Vacquier, V., Steenland, N. C., Henderson, R. G., and Zietz, I., 1951, Interpretation of aeromagnetic maps: Mem. 47, Geol. Soc. Am.
Whittaker, A., Ed., 1985, Atlas of onshore sedimentary basins in England and Wales: Blackie & Sons.
Whittaker, A., Chadwick, R. A., Kirby, G. A., Kubala, M., and Sobey, R. A., 1980, Geological well completion report, Kempsey No. 1 Borehole: Rep. Deep Geol. Unit, Inst. Geol. Sci., 80/2.

APPENDIX
DERIVATION OF STRUCTURAL INDICES

The structural indices for various simple bodies may be derived by direct solution of Euler's equation. The point dipole ($N = 3$), point pole ($N = 2$), line of dipoles ($N = 2$), and line of poles ($N = 1$) have been discussed by Smellie (1956). We examine here the cases of some extended real bodies.

Magnetic anomaly of a thin dike

The vertical magnetic anomaly Z of an infinite thin dike (Bosum, 1968) may be expressed as

$$Z(x, z) = AS/r^2,$$

where

$A = 2Mt \cos \psi,$

$M =$ magnetization intensity,

$t =$ dike thickness $(t \ll z_0)$,

x_0, z_0 are the coordinates of the dike top,

$\cos \psi = [\cos^2 \alpha \cos^2 I + \sin^2 I]^{1/2},$

$\alpha =$ azimuth of profile w.r.t. magnetic north,

$I =$ inclination of geomagnetic field,

$\tan I' = (\tan I)/(\cos \alpha) =$ reduced field inclination,

$S = [-(x - x_0) \sin \beta + (z - z_0) \cos \beta],$

$\beta =$ dip of dike w.r.t. reduced inclination of field, and

$r^2 = (x - x_0)^2 + (z - z_0)^2.$

Then the derivatives are

$$\partial Z/\partial x = -A[r^2 \sin \beta + 2S(x - x_0)]/r^4$$

and

$$\partial Z/\partial z = A[r^2 \cos \beta - 2S(z - z_0)]/r^4.$$

Substitution into the left-hand side of Euler's equation (1) yields

$$(x - x_0)\partial Z/\partial x + (z - z_0)\partial Z/\partial z$$

$$= A\{-(x - x_0) \sin \beta \, r^2 + (z - z_0) \cos \beta \, r^2$$

$$- 2S[(z - z_0)^2 + (x - x_0)^2]\}/r^4$$

$$= A[Sr^2 - 2Sr^2]/r^4$$

$$= -AS/r^2$$

$$= -Z(x, z).$$

If this last result is compared with the right-hand side of equation (1), it is clear that N is 1.0, so that a structural index of 1.0 is correct for the case of the vertical field anomaly of the dipping thin dike. Since the result is independent of the dip of the dike or the earth's field, it is valid for all members of the anomaly family (Gay, 1963) and is therefore also valid for total-field anomalies and includes sill edges (sills may be regarded as dikes with zero dip).

Gravity anomaly of a finite step

The gravity anomaly of a finite step (typically a fault) may be expressed (Jung, 1961) as

$$g(x, z) = 2G\rho[\Phi_0(z - t) - \Phi_u(z - T) + (x - x_0) \ln (R_u/R_0)],$$

where

G is the gravity constant,
ρ is the density contrast,
Φ_0 (or Φ_u) $= \pi/2 + \arctan \{(x - x_0)/[t \text{ (or } T) - z]\}$,
x_0 is the x coordinate of the step midpoint,
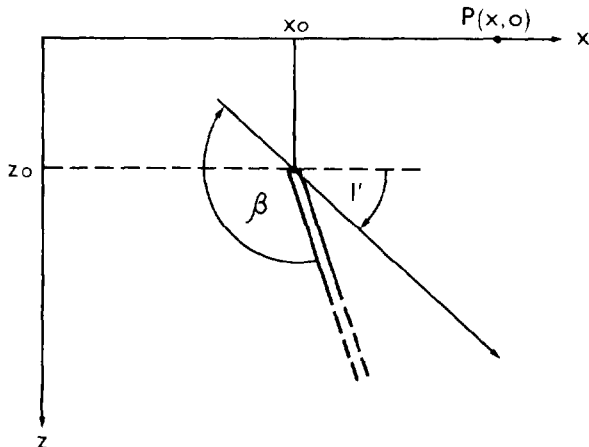$t(T)$ is the depth to the top (bottom) of the step, and

$$R_0 \quad (\text{or } R_u) = \{(x - x_0)^2 + [z - t \text{ (or } T)]^2\}^{1/2}.$$

Then

$$\partial g/\partial x = 2G\rho \ln (R_u/R_0)$$

and

$$\partial g/\partial z = 2G\rho(\Phi_0 - \Phi_u).$$

Substitution into Euler's equation yields

$$(x - x_0)\partial g/\partial x + (z - z_0)\partial g/\partial z$$

$$= 2G\rho[(z - z_0)(\Phi - \Phi_u) + (x - x_0) \ln (R_u/R_0)].$$

This approximates the above expression for $g(x, z)$ provided $t \approx T$ (i.e., depth to step considerably greater than step thickness). It follows that the structural index is unity. The approximation suggests that solution of Euler's equation for the step position should yield the midpoint of the step.

Magnetic anomaly of a sloping contact

The magnetic anomaly (total, vertical, horizontal) of a magnetic contact (often a fault) is given by Am (1972) as

$$F(x, z) = C(\Phi \sin \Theta - \cos \Theta \ln R) + K,$$

where

$C =$ amplitude coefficient,
   $= 2P(F'/F) \sin \delta$ (for total-field anomaly),
$\Phi = \pi/2 + \arctan [(x - x_0)/(z - z_0)]$,
$\Theta =$ combined magnetic angle,
   $= I'(P) + I'(F) - \delta$,
$P =$ polarization vector
$F =$ measurement vector,
P', F' are projections of P, F in the xz plane,
$I'(P), I'(F)$ are inclinations of the projected vectors P', F',
   $\delta =$ dip of contact,
   $R = [(x - x_0)^2 - (z - z_0)^2]^{1/2}$, and
   $K =$ an offset introduced by allowing the lower edge of the step to take an arbitrarily large depth.

Then

$$\partial F/\partial x = C \cos \Theta(x - x_0)/R^2 - C \sin \Theta(z - z_0)/R^2$$
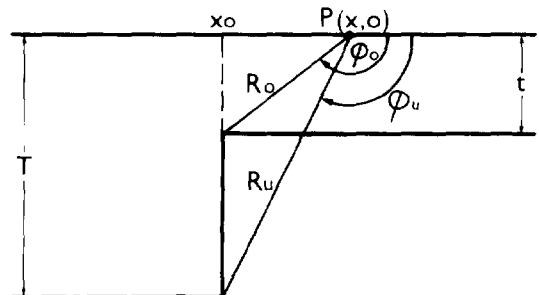
and

FIG. A-1. Magnetic anomaly of a thin dipping dike.

FIG. A-2. Gravity anomaly of a finite dipping step.

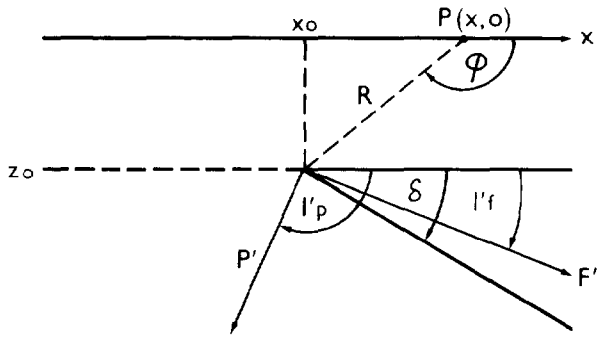FIG. A-3. Magnetic anomaly of a dipping contact.

$$\partial F/\partial z = C \sin \Theta (x - x_0)/R^2 + C \cos \Theta (z - z_0)/R^2.$$

Substitution into Euler's equation yields

$$(x - x_0)\partial F/\partial x + (z - z_0)\partial F/\partial z = C \cos \Theta.$$

This remarkable result implies that the structural index is zero if the combined magnetic angle is 90 degrees. If the combined angle is not zero, a structural index of zero is still valid provided that the least-squares solution of Euler's equation includes solution for an offset whose value combines amplitude, strike, and dip effects.